Journal of Macromolecular Science, Part A
Publication details, including instructions for authors and subscription information:
http://www.informaworld.com/smpp/title~content=t713597274

The Characterization and Thermal Investigation of Chitosan-Fe_3O_4 Nanoparticles Synthesized Via A Novel One-step Modifying Process

Wei Li[a]; Ling Xiao[a]; Caiqin Qin[b]
[a] Department of Environmental Science, College of Resource and Environmental Science, Wuhan University, Wuhan, P.R. China [b] Laboratory for Natural Polysaccharides, Xiaogan University, Xiaogan, P.R. China

Online publication date: 19 November 2010

To cite this Article Li, Wei , Xiao, Ling and Qin, Caiqin(2011) 'The Characterization and Thermal Investigation of Chitosan-Fe_3O_4 Nanoparticles Synthesized Via A Novel One-step Modifying Process', Journal of Macromolecular Science, Part A, 48: 1, 57 — 64
To link to this Article: DOI: 10.1080/10601325.2011.528309
URL: http://dx.doi.org/10.1080/10601325.2011.528309

Journal of Macromolecular Science, Part A: Pure and Applied Chemistry (2011) **48**, 57–64

ISSN: 1060-1325 print / 1520-5738 online
DOI: 10.1080/10601325.2011.528309

Taylor & Francis
Taylor & Francis Group

The Characterization and Thermal Investigation of Chitosan-Fe_3O_4 Nanoparticles Synthesized Via A Novel One-step Modifying Process

WEI LI[1], LING XIAO[1,*] and CAIQIN QIN[1,2]

[1]*Department of Environmental Science, College of Resource and Environmental Science, Wuhan University, Wuhan, P.R. China*
[2]*Laboratory for Natural Polysaccharides, Xiaogan University, Xiaogan, P.R. China*

Received March 2010, Accepted June 2010

A novel modifying process was designed to prepare ultra small magnetic chitosan nanoparticles which exhibited unique thermal stability and decomposition mechanism. The chemical structures and physical properties of the prepared products were characterized using FTIR, TEM, XRD, TGA and DSC techniques. The results revealed that this approach eliminated the aggregation among nanoparticles. The magnetic chitosan particles were 10–15 nm in size with good dispersibility and new thermal property. To further study the decomposition process, the combined TGA-FTIR technique was used to the analysis of the evolution with the temperature of the gas products evolved in the degradation of the magnetic chitosan. The phenomena were observed directly from TGA-FTIR stack plots. From the measurements data, it suggested that the unusual thermal behavior of chitosan might be attributed to the additional bridging through metal oxide.

Keywords: Magnetic nanoparticles, chitosan, microscopic observation, thermal analysis

1 Introduction

With the rapid development of nanotechnology, the synthesis of magnetite nanoparticles (Fe_3O_4) and their composite nanomaterials has attracted both fundamental and practical interest, not only in fundamental properties such as electronic, magnetic, catalytic, and chemicalor biological properties (1–3), but also in technological applications such as high-density magnetic recording media, sensors, catalysts, and clinical uses (4–6). All these applications require that the nanoparticles are superparamagnetic with nanosize and the overall particle size distribution is narrow so that the particles have uniform physical and chemical properties. However, producing magnetic particles with the desired size and acceptable size distribution without particle aggregation has consistently been a problem (7, 8). So, stabilizers such as surfactants, oxide, metal nanoparticles or natural and synthetic polymers with some specific functional groups have been used to increase the stability of these particles (9–11). Chitosan, one of the natural polymer systems, has been intensively studied as a base material for magnetic carriers because of its significant biological and chemical properties (12, 13). In its linear polyglucosamine chains of high molecular weight, chitosan has reactive amino and hydroxyl groups, amenable to chemical modifications. The amino groups make chitosan a cationic polyelectrolyte, one of the few found in nature. When chitosan possesses a high positive charge on –NH3 groups at pH < 6.5, it can effectively aggregate with polyanionic compounds and chelate metal ions (14, 15). Functionalization and modification of the surface with chitosan bring many new functions and applications for the magnetite (16–19).

The conventional method for preparing magnetic chitosan nanoparticles is a two-step modifying process. The first step relies on the synthesis of magnetite nanoparticles. Magnetite is generally prepared mainly by three process, viz., (1) coprecipitation of an aqueous solution of Fe^{2+}/Fe^{3+} in the presence of a base, usually an alkali hydroxide or ammonia; (2) thermal decomposition of an iron complex using an oxidizing agent; and (3) by a sonochemical approach. The second step is based on the formation of the core-shell nanoparticles, in which water/oil or

*Address correspondence to: Ling Xiao, Department of Environmental Science, College of Resource and Environmental Science, Wuhan University, Wuhan 430072, P.R. China. Tel: +86-27-61063891; Fax: +86-27-68763162; E-mail: xiaoling9119@yahoo.cn

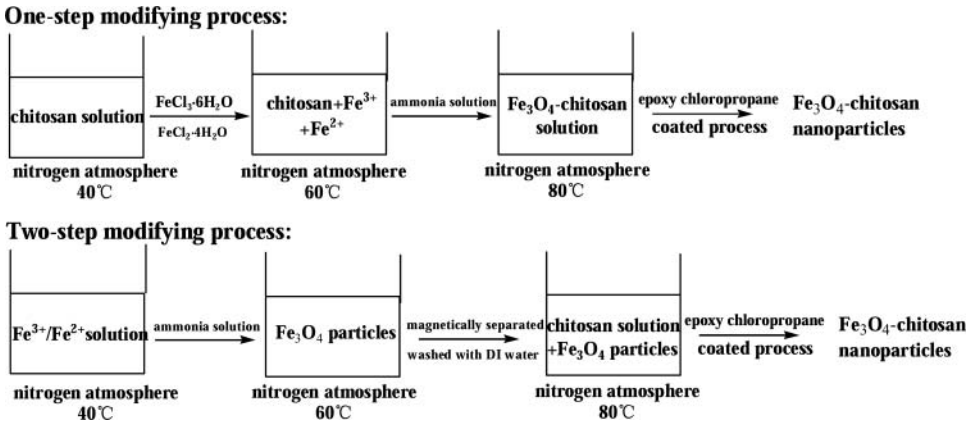

Fig. 1. Preparation procedures of Fe_3O_4-chitosan nanoparticles.

aqueous system, temperature, stirring rate and surfactant are used to confine and control the coating of chitosan on core magnetite (19–23). While a number of approaches to the synthesis of magnetic chitosan nanoparticles have been reported, relatively little have directly observed the core-shell structure and prepared the nanoparticles with sizes smaller than 20 nm and the narrow particle size distribution. From these papers, it could be seen that the magnetic chitosan nanoparticles were aggregated tightly though the size of the magnetite core is nanosize. We hypothesized that this situation was due to the lack of thorough dispersion of magnetite nanoparticles. Before the chitosan was coated on the surface, the magnetite nanoparticles were prone to aggregate and enlarge the particle size. Thus, we sought to use the high adsorption capacity and chelation of chitosan to Fe ions to design a novel modifying process for preparing magnetic chitosan nanoparticles. The obtained magnetic chitosan nanoparticles were characterized by X-ray diffraction (XRD), Fourier transform infrared spectroscopy (FTIR), transmission electron microscopy (TEM) and thermal analysis. The thermal stability and decomposition mechanism of the magnetic chitosan nanoparticles were discussed in detail by DSC, TGA and TGA-FTIR techniques.

2 Experimental

2.1 Materials

Ferric chloride hexahydrate ($FeCl_3 \cdot 6H_2O$, >99%), ferrous chloride tetrahydrate ($FeCl_2 \cdot 4H_2O$, >99%) and ammonium hydroxide (29.4%) were obtained from Tianjing Chemical Reagent Inc. (China). Chitosan with molecular weight of 6.0×10^5 g/mol and 87% of degree of deacetylation was obtained from Lianyungang Biologicals Inc. (China). All other chemicals were of analytic grade reagents and used without further purification.

2.2 Synthesis of Fe_3O_4-Chitosan Nanoparticles

The Fe_3O_4-chitosan nanoparticles were prepared and the general procedures adopted were given in Figure 1. In a two-step modifying process, the Fe_3O_4 nanoparticles were prepared using a co-precipitation method first. These particles were collected and washed several times with distilled water. The calculated amount of Fe_3O_4 was dispersed in acidic chitosan solution with ultrasonication for 30 min. In the one-step modifying process, the ferric and ferrous ions were dispersed in acidic chitosan solution at nitrogen atmosphere. The crosslinking step was similar for the two modifying processes. After being stirred for 20 min at 60°C, ammonium hydroxide and epoxy chloropropane were added dropwise into the solution in 3 h at 80°C. The magnetic chitosan was collected using a magnet and washed consecutively with 0.5% acetic acid and water. The products were then dried in an oven at 60°C for 12 h and kept in a vacuum dessicator for further analysis and use.

2.3 Characterization and Instrumentation

The infrared spectra of all samples were recorded on Nicolet 5700 Fourier transform infrared spectrometer (Nicolet Instrument Co., USA) using KBr pellets. The micrographs with a high magnification were obtained by a JEM-2010 transmission electron microscope machine (JEOL Co., Japan) at an accelerating voltage of 200 kV. The crystal structures of nanoparticles were characterized by D 8 Advance X-ray diffraction (Bruker Co., GER). Particle size was measured by Malvern Zetasizer Nano ZS (Malvern Instruments Ltd., UK). The thermogravimetric analysis was performed at a heating rate of 10°C/min until 850°C on a DuPont Thermal Analyzer 951 (TA Instrument Co., USA), under nitrogen flow of 200 ml/min. The released gases during thermal degradation of the samples were analyzed with the thermogravimetric analyzer coupling with the Fourier transform infrared spectrometer (TGA-FTIR).

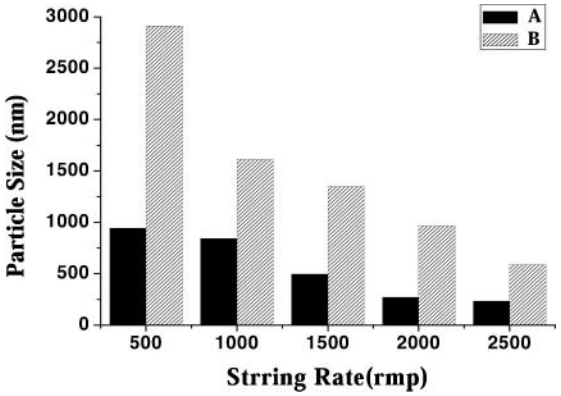

Fig. 2. Effects of stirring rate on the size/size distribution. All formulations were prepared with a Fe/chitosan ratio of 1:1 g/g in one-step (A) and two-step (B) modifying process.

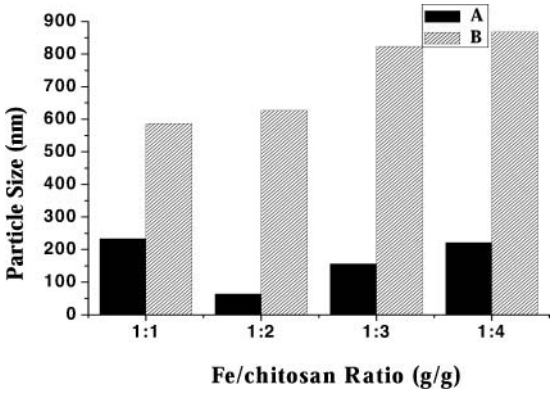

Fig. 3. Effects of the Fe/chitosan ratio on the size/size distribution. The formulations were prepared at 2500 rpm stirring rate in one-step (A) and two-step (B) modifying process.

3 Results and Discussion

3.1 Size and Size Distribution

In this part of the study, the stirring rate of the suspension medium and the Fe/chitosan ratio (g/g) were selected and evaluated as being the most effective parameters determining the size/size distribution of the magnetic chitosan. All samples were dispersed into deionized water with ultrasonication for 5 min before the measurement of the particle size.

The stirring rate of the suspension medium was varied between 500 and 2500 rpm for investigation of the effects of the stirring rate on the size/size distribution. The Fe/chitosan ratio was fixed at 1:1 g/g during the preparation of particles with different stirring rates. The results obtained were shown in Figure 2. It could be seen that the size of the particles decreases with increasing the stirring rate both in one-step and two-step modifying processes. This trend could be explained by the energy transfer differences for the different stirring rates. When the stirring rate was increased, the energy transferred to the suspension medium was increased and the polymer solution could be dispersed into smaller droplets and the size was reduced (24).

The Fe/chitosan ratio was varied in the range 1:1–1:4 (g/g). The stirring rate was fixed at 2500 rpm. The results obtained were shown in Figure 3. It could be seen that the size of the particles increased with increasing chitosan content in a two-step modifying process (Fig. 3B). In the first step of the process, chitosan molecules were adsorbed on the Fe_3O_4 nanoparticles surface. In the second step, the chitosan grafted from the Fe_3O_4 nanoparticles and formed a cross-linked structure on Fe_3O_4 nanoparticles surface. The higher concentration of chitosan resulted in more chitosan cross-linked on the Fe_3O_4 surface. While in one-step modifying process (Fig. 3A), the size of magnetic chitosan was decreased firstly, and then increased with increasing chitosan content. It suggested that the adsorbability and chelation of chitosan molecules to Fe ions could induce Fe_3O_4 particles aggregation. This speculation was approved by the following results of experiments.

3.2 Characterization of Magnetic Chitosan

The functional groups of chitosan were very important for diverse applications, especially for biotechnological purposes. Therefore, the present functional groups should be kept even if the shape was changed into a new form. FTIR spectra were shown in Figure 4 for naked $Fe_3O_4$and magnetic chitosan from a one-step modifying process with different Fe/chitosan ratio. The OH groups of chitosan polymer at 3500^{-1} cm were present in the case of the magnetic chitosan. Two peaks at 2960^{-1} and 2870 cm^{-1}, corresponding to C–H stretching absorptions could be assigned to the cross-linked chitosan (22). These peaks in Figure 4(b and c) were wider and stronger than that in Figure 4(d), demonstrating that the samples b and c carried more chitosan. Domard et al. indicated that characteristic absorptions

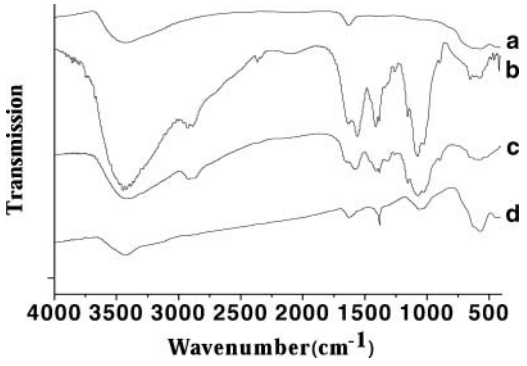

Fig. 4. FTIR spectra of particles: naked Fe_3O_4 (a) magnetic chitosan from one-step modifying process with 1:3 Fe/chitosan ratio (b), 1:2 Fe/chitosan ratio (c) and 1:1 Fe/chitosan ratio (d).

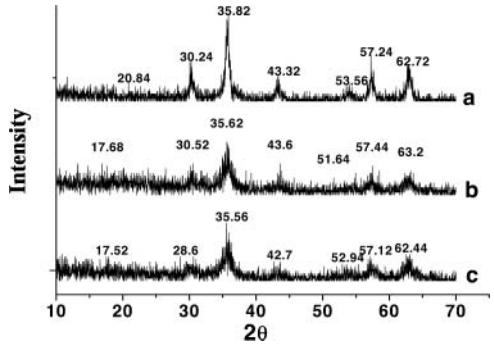

Fig. 5. XRD patterns for magnetic chitosan particles from a one-step modifying process with 1:1 Fe/chitosan ratio (a), 1:3 Fe/chitosan ratio (b) and 1:2 Fe/chitosan ratio (c).

were displayed at 1656.5^{-1} and 1554 cm^{-1} attributable to amide bands I and II in the IR spectrum of chitosan (23). Compared with the spectrum of Figure 4(b and c), it was found that the 1680^{-1} peak shifted to 1661 cm^{-1} and the 1594 cm^{-1} peak shifted to 1578 cm^{-1}. It indicated that the interaction between chitosan and Fe_3O_4 might be changed with the increase of chitosan content in magnetic particles. The characteristic absorption peak for Fe_3O_4 was observed at 576.83 cm^{-1} (Fe–O) for all samples (21).

The crystal structures of magnetic chitosan from a one-step modifying process with different Fe/chitosan ratio were characterized by X-ray diffraction (Fig. 5). The six characteristic peaks for Fe_3O_4 ($2\theta = 30.08^\circ$, 35.42°, 43.08°, 53.56°, 56.98° and 62.62°) marked by their indices ((220), (311), (400), (422), (511) and (440)) were observed for all samples (25). While the broad peak at $2\theta = 17$–21° was ascribed to chitosan that indicated the existence of an amorphous structure(26). From Figure 5(a–c), the broader reflection planes and the change of peaks were perhaps due to decreasing size of the magnetic particles. The magnetic chitosan particles were validated as the binding of chitosan and Fe_3O_4.

TEM micrographs of neat Fe_3O_4 nanoparticles (a) and those coated with chitosan (b-f) were shown in Figure 6. The Fe_3O_4 particles had a tendency to aggregate that might be caused by the coercive forces of magnetite particles. As chitosan was employed, the obtained magnetic particles were small in size that was related to the coated chitosan enhancing the repulsion of magnetite particles (27). By comparing Figure 6c with Figure 6b, the size of magnetic particles from the two-step process became more non-uniform with the increase of chitosan content. It could be seen that the magnetic chitosan nanoparticles were aggregated tightly though the size of the magnetite core was nanosize. This situation was due to the lack of thorough dispersion of magnetite nanoparticles. Before the chitosan was coated on the surface, the magnetite nanoparticles were prone to aggregate and enlarge the particle size.

The magnetic particles with 1:2 Fe/chitosan ratio from a one-step modifying process were nearly spherical in shape

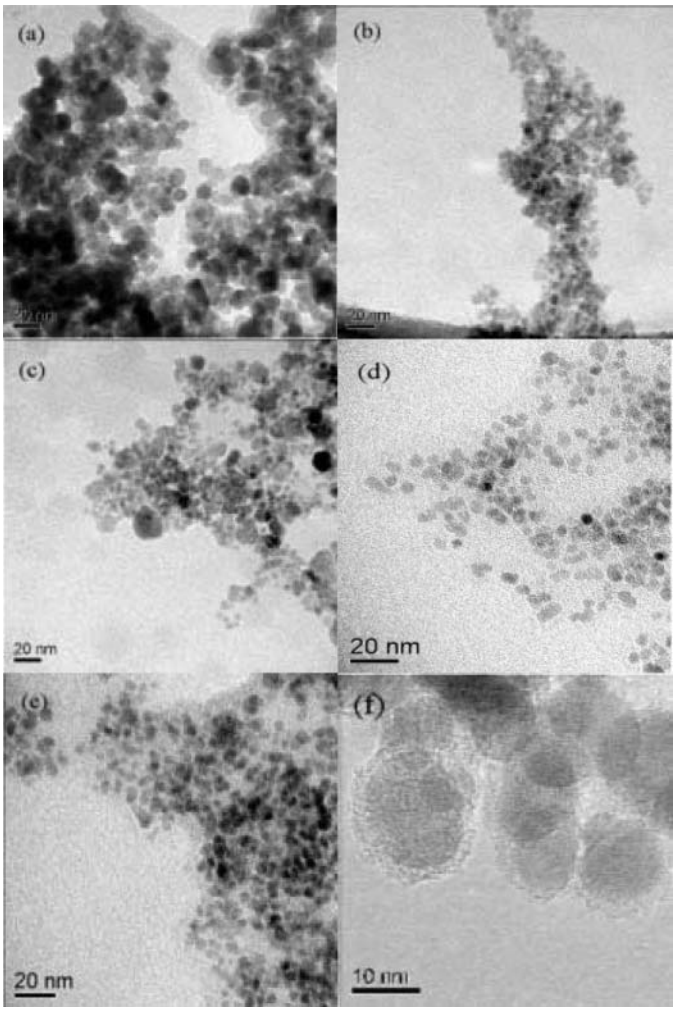

Fig. 6. TEM images of particles: naked Fe_3O_4 (a); magnetic chitosan particles from a two-step modifying process with 1:2 (b) and 1:3 (c) Fe/chitosan ratio; magnetic chitosan particles from one-step modifying process with 1:2 (d), 1:3 (e,f) Fe/chitosan ratio.

and exhibited higher dispersibility (Fig. 6d). The individual nanoparticles appeared to be well isolated. The average particle size was smaller than that from the two-step modifying process. These magnetite particles were prepared in the presence of chitosan during formation, and resulted in a very small particle (about 10–15 nm) with a narrow size distribution. When the ratio (Fe/chitosan) decreased to 1:3 g/g, the magnetic particles from the one-step modifying process (Fig. 6e) were bigger in size. This behavior could be explained by more chitosan crosslinked with an increase in the concentration of chitosan. The results of TEM were consistent with the result of XRD (Fig. 5) and the effects of the Fe/chitosan ratio on the size/size distribution (Fig. 3A). As shown in Fig. 6f, the extra chitosan caused a noticeable change in the particle morphology that a shell with the thickness of 1–1.5 nm was coated evenly on the surface. The inner spheres were the

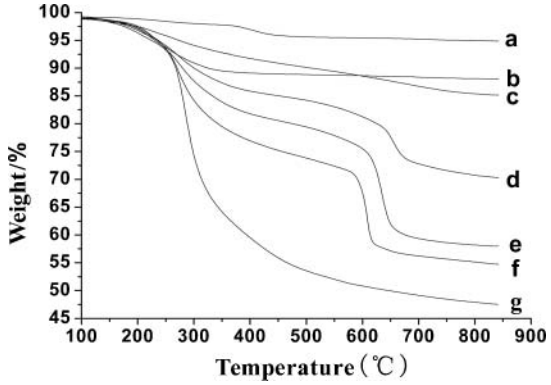

Fig. 7. Thermogravimetric analysis (TGA) of particles: naked Fe_3O_4 (a); magnetic chitosan particles from two-step modifying process with 1:2 Fe/chitosan ratio (b); magnetic chitosan particles from one-step modifying process with 1:1 Fe/chitosan ratio (c), 1:2 Fe/chitosan ratio (d), 1:3 Fe/chitosan ratio (e) and 1:4 Fe/chitosan ratio (f); cross-linked chitosan (g).

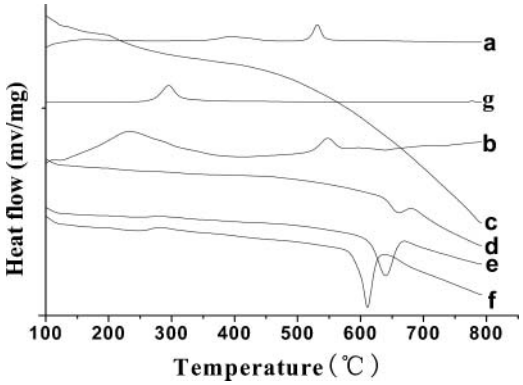

Fig. 8. Differential scanning calorimetry (DSC) of particles: naked Fe_3O_4 (a); magnetic chitosan particles from two-step modifying process with 1:2 Fe/chitosan ratio (b); magnetic chitosan particles from one-step modifying process with 1:1 Fe/chitosan ratio (c), 1:2 Fe/chitosan ratio (d), 1:3 Fe/chitosan ratio (e) and 1:4 Fe/chitosan ratio (f); cross-linked chitosan (g).

chitosan/Fe_3O_4 composite because the chitosan content of these particles was about 42%, according to the weight loss in Figure 7e. The dark spots which correspond to the metallic core were not clearly observed that indicated the Fe_3O_4 evenly dispersed in the polyglucosamine chains of chitosan (1).

3.3 Thermal Decomposition of Magnetic Chitosan

The TGA and DSC curves of Fe_3O_4 and magnetic chitosan particles were shown in Figures 7 and 8, respectively. For naked Fe_3O_4, the TGA curve (Fig. 7a) showed that the weight loss over the temperature range from 100 to 850°C was about 2%. This might be due to the loss of residual water. The cross-linked chitosan had a high speed of decomposition between 250–450°C (Fig. 7g), with an exothermic-peak at 290°C (Fig. 8g). This effect was also associated to a mass loss (46.4%) which was attributed to the degradation and interchain crosslink of the composite. The pyrolysis of polysaccharide structure started by a random split of the glycosidic bonds, followed by a further decomposition forming acetic and butyric acids and a series of lower fatty acids (28, 29). For the magnetic chitosan particles from the two-step modifying process with 1:2 Fe/chitosan ratio, the weight loss was about 12% from 220 to 400°C (Fig. 7b). It was apparent that this degradation stage of sample b was mainly the cross-linked chitosan component on the Fe_3O_4 nanoparticle surface, after comparing its TGA and DSC curves with sample a and g's. According to the literature, the final temperature of decomposition for the magnetic chitosan particles with different chitosan content which were prepared from the traditional two-step modifying process was around 350–450°C (20, 30).

The magnetic chitosan particles from one-step modifying process with 1:1 Fe/chitosan ratio had a mild speed of decomposition during the temperature of 240 and 680°C (Fig. 7c). When the Fe/chitosan ratio decreased to 1:2, the curves of the magnetic chitosan were changed. A new weight loss appeared between 640 and 680°C (Fig. 7d). This second degradation stage with weight loss of 12.7% occurred endothermically, as pointed out by the DSC profile (Fig. 8d). From the results of thermal analysis, one could note an increase in weight loss and a shift to a lower temperature for the second degradation stage that was attributed to a decrease in thermal stability as a consequence of an increase in chitosan content of particles (Fig. 7d–f). Because of their similar composition and structure, the magnetic chitosan particles with different chitosan content showed the similar endothermic peaks (Fig. 8 d–f).

3.4 TGA-FTIR Analysis

The above decomposition phenomena could be observed from the stack plots of the coupling TGA and FTIR measurements by analyzing the gas spectra from the decomposition of the samples. The combination of these two techniques permits a complete characterization of materials in terms of thermal stability and decomposition mechanisms. Figure 9 showed the (a) stack plots of cross-linked chitosan, (b) magnetic chitosan particles from two-step modifying process and (c). magnetic chitosan particles from one-step modifying process with 1:2 Fe/chitosan ratio These on-line FTIR spectras corresponding to the products generated in the TGA furnace were obtained during the temperature of 580 and 680°C under nitrogen. As could be seen in Figure 9a, the infrared spectra showed water peaks (at 1628–1541 $cm^{-1}$and 3735–3526 cm^{-1}) and CO_2 peaks (at 670 and 2359–2311 cm^{-1}) (31, 32). Figure 9b, with the lower volume of released gases, was similar to Fig. 9a.

In Figure 9c, a new peak island appeared between 2158 and 2120 cm^{-1}, indicated the existence of CO among the

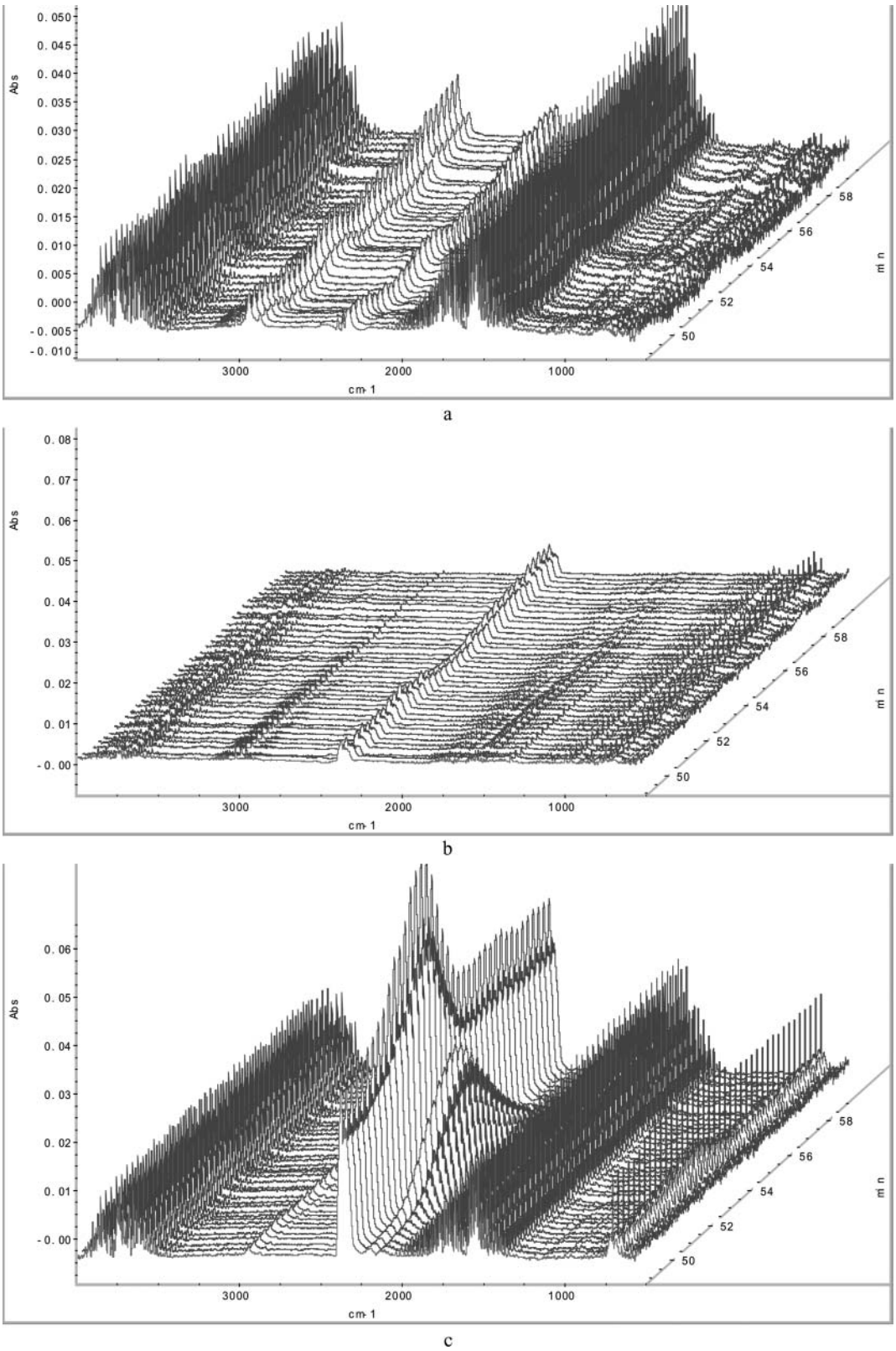

Fig. 9. (a)TGA-FTIR stack plots of cross-linked chitosan, (b) magnetic chitosan particles from two-step modifying process with 1:2 Fe/chitosan ratio and, (c) magnetic chitosan particles from a one-step modifying process with 1:2 Fe/chitosan ratio during the temperature of 580 and 680°C.

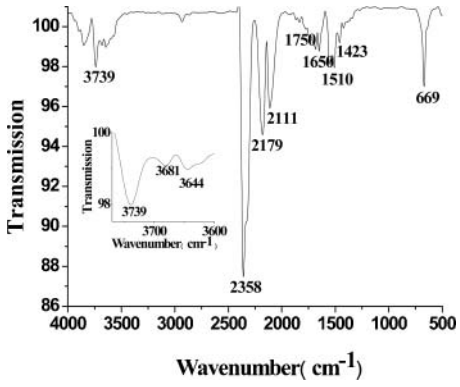

Fig. 10. FTIR spectra of the magnetic chitosan particles from a one-step modifying process with 1:2 Fe/chitosan ratio at 640°C.

gases detected by IR probe (32). This island started at around 620°C, and ended at around 660°C, which corresponded to the weight loss of the second stage in Fig. 7d. For the purpose of analyzing the evolution with the temperature of the qualitative composition in the oxidative degradation process, the FTIR spectra at 640°C corresponding to the gas evolved from the magnetic chitosan particles had been extracted from the stack plots. Figure 10 showed this FTIR spectra, providing confirmation that the major decomposition products were H_2O (1650 cm^{-1}, 3739 cm^{-1}), NH_3 (1423 cm^{-1}, 3644 cm^{-1}, 3681 cm^{-1}), CO_2(669 cm^{-1}, 1750 cm^{-1}, 2358 cm^{-1}) and CO (2111 cm^{-1}, 2179 cm^{-1}) (33, 34). For the abrupt change of CO_2 volume from 620 to 66°C (appeared at around 2400 cm^{-1}), it could be explained by that the cleavage reaction of the polymer chain might be completed while the oxidation was still going on (35). However, the continuing NH_3 and new hump caused by a amount of CO suggested the cleavage and then oxidation of the segment of chitsoan chain, which chelated with Fe ions before the Fe_3O_4 particles formed.

The enhanced thermal stability of cross-linked chitosan might be due to the effect of two factors: (a) conformational changes of chitosan, and (b) additional bridging between metal particles and chitosan. Here, we propose a formation mechanism of the magnetic chitosan particles from one-step modifying process (Fig. 11). Fe^{2+}/Fe^{3+} ions penetrated into the polyglucosamine chains of chitosan by diffusion effect in acid solution firstly. With increasing pH to 5–6, these ions chelated with the functional group on the chitsoan chain. Then magnetic chitosan particles were obtained by alkaline co-precipitation of Fe^{2+} and Fe^{3+}. The electrostatic interaction and chelation of chitosan to the ions could be effectively promote the nucleation of Fe_3O_4 and reduce particle aggregation. Chelation was known to change the conformation of the chitosan polymer. Disturbance of the natural ordering of the polymer might be expected to lead to thermal instability, while the additional bridging through metal ion or oxide might be expected to lead to enhancement of thermal stability. The increase in the decomposition temperature of the complexes was considered to be a measure of these two opposing factors (36, 37).

4 Conclusions

In this work, we have demonstrated a one-step modifying process for preparing magnetic chitosan, which is different from the processes reported previously. In addition to the evidence from FTIR spectra, the change of size distribution and XRD detection of the diffraction peaks for magnetic chitosan with different chitosan content, the formation and morphology of the chitosan/Fe_3O_4 nanoparticles was

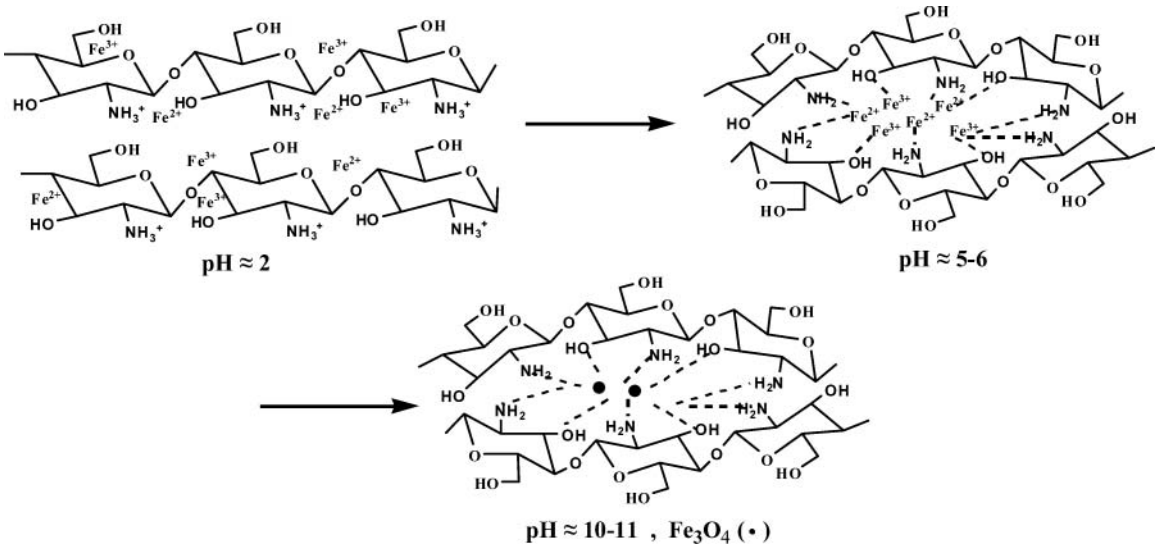

Fig. 11. A schematic showing the formation mechanism of the magnetic chitosan particles from one-step modifying process.

further confirmed by TEM analysis. A shell of chitosan, with a thickness found to be 1–1.5 nm, was coated evenly on the magnetic chitosan. These combined results have demonstrated the controllability of size and composition for the synthesis of the nanoparticles. In order to explain the unique thermal stability and decomposition mechanism of the magnetic chitosan from the novel modifying process, an experimental work on the thermal degradation and pyrolysis was conducted with the aid of the combined TGA-FTIR. The results suggested that their unusual decomposition behaviors might be attributed to the stability of the segment of chitsoan chain which chelated with Fe ions before the Fe_3O_4 particles formed. The additional bridging through metal oxide might be expected to lead to enhancement of thermal stability. Meanwhile, this chelation effect could homogeneously disperse the Fe ions into the polyglucosamine chains of chitosan and reduce particle aggregation during the modifying process.

Acknowledgement

This work was supported in part by the National Natural Science Foundation of China (30571462).

References

1. Tartaj, P., Morales, M.P., Gonzalez-Carreno, T., Veintemillas-Verdaguer, S. and Serna, C.J. (2005) *J. Magn. Magn. Mater*., 290–291, 28–34.
2. Perez, J.M., Simeone, F.J., Saeki, Y., Josephson, L. and Weissleder, R. (2003) *J. Am. Chem. Soc.*, 125(34), 10192–10193.
3. Kim, E.H., Lee, H.S., Kwak, B.K. and Kim, B-K. (2005) J. Magn. Magn. Mater., 289, 328–330.
4. Berry, C.C. and Curtis, A.S.G. (2003) *J. Phys. D: Appl. Phys*., 36, 198–206.
5. Zhang, Y., Kohler, N. and Zhang, M. (2002) *Biomaterials*, 23, 1553–1561.
6. McCarthy, J.R. and Weissleder, R. (2008) *Adv. Drug Delivery Rev.,* 60, 1241–1251.
7. Caruso, F., Spasova, M., Susha, A., Giersig, M. and Caruso, R.A. (2001) *Chem. Mater.,* 13, 109–116.
8. Sun, S. and Zeng, H. (2002) *J. Am. Chem. Soc*., 124(28), 8204–8205.
9. Woo, K., Hong, J., Choi, S., Lee, H-W. and Ahn, J-P. (2004) *Chem. Mater.,* 16, 2814–2818.
10. Marinescu, G., Patron, L., Culita, D.C. and Neagoe, C. (2006) *J. Nanopart. Res*., 8, 1045–1051.
11. Zhu, A., Yuan, L. and Liao, T. (2008) *Int. J. Pharm*., 350, 361–368.
12. Harish Prashanth, K.V. and Tharanathan, R.N. (2007) *Trends Food Sci. & Technol*., 18, 117–131.
13. Varmaa, A.J., Deshpandea, S.V. and Kennedy, J.F. (2004) *Carbohydr. Polym*., 55, 77–93.
14. Guibal, E. (2004) *Sep. Purif. Technol*., 38, 43–74.
15. Chassary, P., Vincent, T. and Guibal, E. (2004) *React. Funct. Polym*., 60, 137–149.
16. Yuan, Q., Venkatasubramanian, R., Hein, S. and Misra, R.D.K. (2008) *Acta Biomater*., 4, 1024–1037.
17. Kaushik, A., Khan, R., Solanki, P.R., Pandey, P. and Alam, J. (2008) *Biosens. Bioelectron*., 24, 676–683.
18. Zhao, G., J.-J., Xu, and Chen, H-Y. (2006) *Electrochem. Commun*., 8, 148–154.
19. Kim, E.H., Ahn, Y. and Lee, H.S. (2007) *J. Alloys Compd*., 434–435, 633–636.
20. Pan, C., Hu, B., Li, W., Sun, Y., Ye, H. and Zeng, X. (2009) *J. Mol. Catal. B: Enzym*., 61, 208–215.
21. Li, G-Y., Jiang, Y-R., Huang, K-L., Ding, P. and Yao, L-L. (2008) *Colloids Surf., A: Physicochem. Eng. Aspects*, 320, 11–18.
22. Zhou, Y-T., Nie, H-L., Branford-White, C., He, Z-Y. and Zhu, L-M. (2009) *J. Colloid Interface Sci*., 330, 29–37.
23. Zhao, D.-L., Wang, X-X., Zeng, X.-W., Xia, Q-S. and Tang, J-T. (2009) *J. Alloys Compd*., 477, 739–743.
24. Denkbas, E.B., Kilicay, E., Birlikseven, C. and Ozturk E., (2002) *React. Funct. Polym*., 50, 225–232.
25. Zhang, J., Xu, S. and Kumacheva, E. (2004) *J. Am. Chem. Soc*., 126(25), 7908–7914.
26. Kang, H-M., Cai, Y-L. and Liu, P.-S. (2006) *Carbohydr. Res*., 341, 2851–2857.
27. de Moura, M.R., Aouada, F.A. and Mattoso, L.H.C. (2008) *J. Colloid Interface Sci*., 321, 477–483.
28. Neto, C.G.T., Giacometti, J.A., Job, A.E., Ferreira, F.C., Fonseca, J.L.C. and Pereira, M.R. (2005) *Carbohydr. Polym*., 62, 97–103.
29. Ostrowska-Czubenko, J. and Gierszewska-Druzynska, M., (2009) *Carbohydr. Polym*., 77, 590–598.
30. Li, G-Y., Jiang, Y.R., Huang, K-L., Ding, P. and Chen, J. (2008) *J. Alloys Compd*., 466, 451–456.
31. Paama, L., Pitkänen, I., Halttunen, H. and Perämäki, P. (2003) *Thermochim. Acta*, 403, 197–206.
32. Huang, N. and Wang, J. (2009) *J. Anal. Appl. Pyrolysis*, 84, 124–130.
33. Hornsby, P.R. and Wang, J. (1996) *Polym. Degrad. Stab*., 51, 235–249.
34. Marcilla, A., Gomez-Siurana, A. and Menargues, S. (2005) *Thermochim. Acta*, 438, 155–16.
35. Wang, J., He, C. and Lin, Y. (2002) *Thermochim. Acta*, 381, 83–92.
36. Herna'ndez, R.B., Franco, A.P., Yola, O.R., Lo'pez-Delgado, A., Felcman, J., Recio, M.A.L. and Mercê, A.L.R. (2008) *J. Mol. Struct*., 877, 89–99.
37. Sreenivasan, K. (1996) *Polym. Degrad. Stab.,* 52, 85–87.